Key role of PIN1 in telomere maintenance and oncogenic behavior in a human glioblastoma model

JULIÁN MAGGIO[1], GEORGINA A. CARDAMA[2], ROMINA G. ARMANDO[1], LARA BALCONE[1], NATASHA T. SOBOL[3], DANIEL E. GOMEZ[1*] and DIEGO L. MENGUAL GÓMEZ[1*]

[1]Molecular Oncology Unit, [2]Antitumor Drug Evaluation and Development Unit and [3]Translational Oncology Unit, Center of Molecular and Translational Oncology, Department of Science and Technology, National University of Quilmes, Bernal, Buenos Aires B1876BXD, Argentina

Received October 20, 2022; Accepted January 20, 2023

DOI: 10.3892/or.2023.8528

Abstract. PIN1 is the only known enzyme capable of recognizing and isomerizing the phosphorylated Serine/Threonine-Proline motif. Through this mechanism, PIN1 controls diverse cellular functions, including telomere maintenance. Both PIN1 overexpression and its involvement in oncogenic pathways are involved in several cancer types, including glioblastoma (GBM), a lethal disease with poor therapeutic resources. However, knowledge of the role of PIN1 in GBM is limited. Thus, the present work aimed to study the role of PIN1 as a telomere/telomerase regulator and its contribution to tumor biology. PIN1 knockout (KO) LN-229 cell variant using CRISPR/Cas9 was developed and compared with PIN1 LN-229 expressing cells. To study the effect of PIN1 absence, status of NF-κB pathway was evaluated by luciferase reporter gene assay and quantitative PCR. Results revealed that PIN1 deletion in GBM cells diminished the active levels of NF-κB and decrease the transcription of il-8 and htert genes. Then, telomere/telomerase related processes were studied by RQ-TRAP assay and telomere length determination by qPCR, obtaining a reduction both in telomerase activity as in telomere length in PIN1 KO cells. In addition, measurement of SA β-galactosidase and caspase-3 activities revealed that loss of PIN1 triggers senescence and apoptosis. Finally, migration, cell cycle progression and tumorigenicity were studied by flow cytometry/western blot, Transwell assay and *in vivo* experiments, respectively. PIN1 deletion decreased migration as well as cell cycle progression by increasing doubling time and also resulted in the loss of LN-229 cell ability to form tumors in mice. These results highlight the role of PIN1 in telomere homeostasis and GBM progression, which supports PIN1 as a potential molecular target for the development of novel therapeutic agents for GBM treatment.

Correspondence to: Dr Diego L. Mengual Gómez, Molecular Oncology Unit, Center of Molecular and Translational Oncology, Department of Science and Technology, National University of Quilmes, Laboratory 11, 352 Roque Saenz Peña, Bernal, Buenos Aires B1876BXD, Argentina
E-mail: diego.mengualgomez@unq.edu.ar

*Contributed equally

Key words: glioblastoma, PIN1, telomere, telomerase, tumorigenicity, molecular oncology

Introduction

The family of adult-type diffuse glioma constitutes the most common tumors of the central nervous system (1). The World Health Organization (WHO) classifies these tumors based on the presence of certain biomarkers and histological characteristics (1). Within this family, glioblastoma multiforme (GBM) is a highly aggressive grade 4 tumor with elevated mitotic activity, vascularization and necrosis (1). The molecular characteristics that define this disease are: Wild-type isocitrate dehydrogenase (IDH) enzymes, mutation in the telomerase reverse transcriptase (*Tert)* promoter, the combination of gain of chromosome 7 and loss of chromosome 10 and epidermal growth factor receptor amplification (2). GBM is considered one of the most lethal tumors in humans. Patients with recurrent GBM have only a 1 year life expectancy after diagnosis with a median survival time of 3-9 months (3). Despite therapeutic efforts, chemotherapy and surgical advances, there is currently no cure for GBM (4).

The main challenges of GBM are its intracranial location combined with fast growth and infiltrative nature that lead to difficult complete surgical resection; another key issue is the development of therapy resistance caused by high genetic instability (5). This instability generates cell populations resistant to conventional therapies that non-specifically target dividing cells. Consequently, novel therapeutic strategies based on targeted therapies are required to improve patient outcomes (5).

PIN1 is linked to tumor development and progression and is commonly overexpressed or overactivated in numerous types of cancer, including GBM (6,7). Atabay *et al* (8) reported that GBM U251 cells with PIN1 knockdown, have revealed that the downregulation of this protein induces apoptosis and also decreases cell proliferation and migration. Therefore, PIN1 is a potential molecular target for GBM treatment (8).

PIN1 is an 18 kDa protein that contains two functional domains: N-terminal WW domain capable of binding specifically to phosphorylated Serine/Threonine-Proline domains and a C-terminal peptidyl-prolyl isomerase domain, which catalyzes cis/trans proline isomerization. It is through this isomerization mechanism that PIN1 is able to generate modifications in a protein after being phosphorylated. Such modifications cause a conformational change that affects the target protein by promoting its activation or inhibition, modifying its folding, altering intracellular location, increasing its stability or promoting its degradation and altering which proteins it interacts with (9,10). By these mechanisms, PIN1 can regulate cellular processes and signaling pathways, including Wnt/β-catenin, c-MYC and NF-κB (11-14). PIN1 inhibition has been reported to decrease activation of NF-κB pathway and its effectors in a GBM cell model (11). NF-κB is a transcription factor that serves a key role in regulating expression of many genes, including inducible and constitutive IL-8 (15). Furthermore, it has been reported that treatment of U251 GBM cells with IL-8 increases the invasive potential of this cell line (16). In line with this, downregulation of NF-κB activity decreases GBM cell invasion, partly mediated by a decrease in IL-8 transcription (17). PIN1 has been reported to regulate cellular processes such as proliferation, invasion/metastasis, angiogenesis, cell death resistance, immune system evasion, cell cycle progression, metabolism and replicative immortality (7).

One of the main characteristics of tumor cells is replicative immortality (18). In a non-pathological context during normal cell division, replicative machinery duplicates each chromosome incompletely, resulting in telomere shortening. Telomeres are nucleoprotein structures found at the ends of each chromosome with the function of maintaining genomic stability. Telomeres constitute repeated DNA sequences joined to a protein complex called sheltering composed of telomeric repeat binding factor (TRF) 1 and 2, protector of telomeres 1, proteins that associate with these telomeric DNA binding actors as TRF1-interacting protein 2, Repressor/activator protein 1 and telomere protection protein 1 (18). Telomere sequence shortens with each cell replication event. This process is essential for tissue degeneration and aging in somatic cells, and its correct functioning prevents malignant cell transformation (19). The major mechanism by which tumor cells achieve unlimited replication is through telomerase enzyme expression (20). Telomerase is a ribonucleoprotein and; its main components are the catalytic subunit human TERT (*htert*) and human telomerase RNA (*hTR*) which acts as a primer for the addition of telomeric sequences at the DNA 3' end (20).

PIN1 modulates telomere maintenance via TRF1, one of the main components of sheltering, by regulating the half-life of this protein. Accordingly, the inhibition of PIN1 prevents the degradation of TRF1, resulting in its accumulation in telomeres (21). This blocks access to telomerase, causing progressive telomere shortening (21). One of the genes regulated by NF-κB pathway, and therefore by PIN1, is *htert*, which serves a key role in replicative immortality caused by telomere elongation in tumor cells (20). In addition, in a leukemia cell model, PIN1 regulates expression of *htert* by activating NF-κB signaling (22). PIN1 inhibition may be involved in telomere maintenance in GBM not only by TRF1 modulation but also by altering *htert* expression and telomerase activity.

Several reports describe the role of PIN1 in cancer development, both for its role in regulating signaling pathways and its ability to modulate telomeric stability (7,8,15,21). Although these processes have been identified in GBM, there is little information on their association with PIN1 in this disease (23,24). Therefore, the present study aimed to determine the role of PIN1 in telomere maintenance and GBM tumor progression, considering this protein and its molecular mechanism may be an attractive target for the development of novel therapies.

Materials and methods

Cell lines and culture. Human GBM cell line LN-229 was purchased from the American Type Culture Collection (cat. no. CRL-2611). Cells were cultured and maintained at 37˚C as a monolayer with DMEM (Thermo Fisher Scientific, Inc.) supplemented with 10% fetal bovine serum (FBS, Sigma Aldrich; Merck KGaA) previously inactivated by heat, 2 mM glutamine and 80 mg/ml gentamicin in a 5% CO_2 atmosphere. Cell cultures were routinely subcultured twice a week by trypsinization according to the manufacturer's instructions.

For the relative determination of telomeric length, senescence and apoptosis, cells at ≥9 passages were used. For *in vivo* tumor progression assay, cells at <6 passages were used.

CRISPR/Cas9-PIN1 plasmid cloning. Specific oligonucleotides for Pin1 gene as guide RNAs (sgRNA) were in house designed to target exon 1 using CRISPRon software v1.0 (25), corresponding to ww domain of PIN1 protein. Sequences were as follows: Forward, 5'-CACCGCATCACTAACGCC AGCCAG-3' and reverse, 5'-AAACCTGGCTGGCGTTAG TGATGC-3'. The commercial plasmid Thy-1-CRISPR-gRNA #2-(pSpCas9(BB)-2A-Puro (PX459) V2.0) (cat. no. #124284; Addgene, Inc.) was used as the backbone for the CRISPR-PIN1 plasmid construction, according to the manufacturer's protocol. Briefly, plasmid digestion was performed using *Bbs*I enzyme. The ligation product was transfected into TOP10 electrocompetent bacteria, and transformed bacteria were grown on a plate with Luria-Bertani medium with ampicillin as selection pressure at 10 μg/ml for selection and maintenance. Plasmid amplification was performed from a positive clone. Correct ligation was confirmed by observing the digestion pattern of double plasmid digestion (*Bbs*I and *Age*I).

LN PIN1 KO cell line generation. Following CRISPR-PIN1 plasmid construction, transfection was performed using TransIntro™ reagent (TransGen Biotech Co., Ltd.) according to the manufacturer's instructions with 1 μg of DNA and $5x10^5$ LN-229 seeded in a 6-well plate at 37˚C for 6 h.

The selection process was performed 48 h after transfection. For selecting cells containing the plasmid, 2 μg/ml puromycin (Thermo Fisher Scientific, Inc.) was added to DMEM with 10% FBS for 5 days. After that, the surviving cells were cultured without puromycin (DMEM 10% FBS) for the development of subsequent experimentation. Surviving cells were cultured without puromycin (DMEM 10% FBS) for the development of subsequent experimentation.

LN PIN1 KO validation by flow cytometry. LN-229 and LN PIN1 KO cells were harvested by trypsinization, collected by centrifugation (5 min at 250 x g) and resuspended in PBS. Cells were fixed with 4% paraformaldehyde in PBS and 1% FBS (Thermo Fisher Scientific, Inc.) for 15 min at 4˚C. Then, cells were permeabilized using a 0.1% PBS-Tween solution with 1% FBS for 30 min at room temperature. Cells were collected by centrifugation (5 min at 250 x g at room temperature) and resuspended in 50 μl PBS with anti-PIN1 antibody (cat. no. sc-46660; Santa Cruz Biotechnology, Inc.; 1:50) and incubated for 30 min at room temperature. After washing with PBS, cells were incubated for 30 min at 4˚C in dark with the secondary FITC anti-mouse IgG2a (cat. no. 562028; BD Pharmingen; BD Biosciences, 1:100) and resuspended in 200 μl PBS. Data were collected and analyzed with BD FACSCalibur cytometer and FlowJo7.6.2 software (BD Biosciences).

Western blotting. For protein extraction, $1x10^6$ LN-229 and LN PIN1 KO were lysed using RIPA buffer with protease inhibitor (Sigma Aldrich; Merck KGaA). The isolated protein was quantified by BCA assay. A total of 20 μg/lane total proteins were analyzed by western blotting to determine protein levels of PIN1 for LN PIN1 KO validation, and Cyclin D1 for cell cycle analysis. A 10% polyacrylamide gel was used and proteins were transferred to a PDVF membrane, which was blocked using a suspension of milk powder in 0.1% TBS-T at room temperature for 1 h. Then, the membrane was incubated overnight at 4˚C with primary anti-PIN1 (cat. no. sc-46660; Santa Cruz Biotechnology, Inc.; 1:500), anti-Cyclin D1 (kindly provided by Dra. MF Rubio; cat. no. sc-718; Santa Cruz Biotechnology, Inc.; 1:1,500) and anti-β-tubulin as loading control (cat. no. 22833; Thermo Fisher Scientific, Inc.; 1:5,000). Following three 0.1% TBS-T washes, bands were visualized using a horseradish peroxidase-conjugated secondary anti-mouse antibody (cat. no. 1662408EDU; Bio-Rad Laboratories, Inc.: 1:10,000) with a bioluminescence kit (Productos Bio-Lógicos) in a C-digit blot scanner with Image Studio software v5.2.5 (LI-COR Biosciences).

Determination of active levels of NF-κB. To evaluate the status of NF-κB in LN PIN1 KO cells, the active levels of this protein were determined using a commercial plasmid, pHAGE NFKB-TA-LUC-UBC-tdTomato-W (Addgene, Inc.; cat. no. 49335). $1x10^5$ LN-229 and LN PIN1 KO cells were transfected in 24-well plates with this plasmid using TransIntro™ transfection reagent (TransGene), according to the manufacturer's instructions with 500 ng of DNA at 37˚C for 6 h. At 72 h post-transfection, induction of the NF-κB pathway was performed, at 37˚C by adding 10 ng/ml LPS (Sigma Aldrich; MercK KGaA). After 6 h, luciferin (Sigma Aldrich; MercK KGaA) was added to the culture medium at 0.1 mM for 10 min at room temperature; luminescence associated with active levels of NF-κB was measured using Cytation 5 plate reader with Gen5 software v3.11 (Biotek Instruments Inc.).

RNA extraction and copy (c)DNA synthesis. Total RNA was isolated from LN-299 and LN PIN1 KO cells using BioZol (Productos Bio-Lógicos), according to the manufacturer's protocol. The extracted RNA concentration and purity were determined with NanoDrop 1000 (Thermo Fisher Scientific, Inc.) spectrophotometer by calculating the ratio of optical density at wavelengths of 260/280 and 260/230 nm. cDNA was synthesized from 1 μg total RNA in 20 μl reaction volume using oligodT18 (Productos Bio-Lógicos) and Superscript III (Thermo Fisher Scientific, Inc.) according to the manufacturer's instructions.

Reverse transcription-quantitative (RT-q)PCR of IL-8, htert and cyclin D1. *IL-8*, *htert* and *cyclin D1* specific primers were designed using Primer Express® Software Version 3.0 (Thermo Fisher Scientific, Inc.). The assay was performed on StepOne™ System using SYBR-Green detection reagent (both Thermo Fisher Scientific, Inc.). *β-actin* was used as a loading control. Analysis of relative gene expression data was performed by the ΔΔCq method (26). Sequences of primers were as follows: *htert* forward, 5'-CTACTCCTCAGGCGACAAGG-3' and reverse, 5'-TGGAACCCAGAAAGATGGTC-3'; *β-actin* forward, 5'-GGACTTCGAGCAAGAGATGG-3' and reverse, 5'-AGGAAGGAAGGCTGGAAGAG-3'; *il-8* forward, 5'-TAAAAAGCCACCGGAGCACT-3' and reverse, 5'-ATCAGGAAGGCTGCCAAGAG-3' and *cyclin D1* forward, 5'-TGGTGAACAAGCTCAAGTGG-3' reverse, 5'-CTGGCATTTTGGAGAGGAAG-3'. Thermocycling conditions were as follows: 10 min at 95˚C for initial denaturation, followed by 40 cycles of PCR (95˚C for 15 sec and 60˚C for 1 min).

Telomerase activity determination. Telomerase activity was determined by real-time quantitative telomerase repeat amplification protocol (RQ-TRAP) assay using SYBRGreen (StepOne™ System; Thermo Fisher Scientific, Inc.). LN-229 and LN PIN1 KO cells ($2x10^6$) were first washed with PBS and centrifuged at 450 x g for 8 min at room temperature in a 1.5 ml Eppendorf tube. The pellets were resuspended in 200 µl of CHAPS {[3-(3-Cholamidopropyl) dimethylammonio-1-propanesulfonate]} lysis buffer at 0.5% p/v with RNaseOUT (Thermo Fisher Scientific, Inc.) and protease inhibitor (Sigma Aldrich; MercK KGaA). Protein concentration was measured by Micro BCA Protein Assay kit (Thermo Fisher Scientific, Inc.) according to the manufacturer's instructions and stored at -20˚C until use.

Briefly, telomerase activity was measured in a final volume of 10 μl, using 2 μl lysate as a template, Power SYBR Green Master Mix 1X (Thermo Fisher Scientific), 250 nM alternative complementary (ACX) primer (5'-GCGCGGCTTACCCTTACCCTTACCCTAACC-3') and 800 nM telomerase substrate (TS) primer (5'-AATCCGTCGAGCAGAGTT-3'). First, 20 min incubation at 25˚C was performed for telomerase mediated extension of the TS primer. Samples were subjected to an initial denaturation at 90˚C for 10 min, followed by 40 cycles of PCR (95˚C for 15 sec and 60˚C for 10 sec). Finally, the reaction ended with melt curve analysis with a linear increase in temperature of 0.2˚C/sec from 55 to 95˚C. StepOne Software v2.3 (Thermo Fisher Scientific, Inc.) was used to analyze results (27).

Relative telomere length determination. Telomere length was evaluated according to the protocol for telomere measurements by qPCR described by Cawthon (28). Pure gDNA kit (Productos Bio-Lógicos) was used to extract high molecular weight DNA from LN-229 and LN PIN1 KO cells, according to the manufacturer's protocol. Extracted DNA was quantified

at 230, 260 and 280 nm absorbance using NanoDrop 1000 (Thermo Fisher Scientific, Inc.) spectrophotometer. Specific primers for the repetitive telomere sequence were used to quantify telomere length. To determine the genome copies on the samples specific primers for the single copy gene ribosomal protein lateral stalk subunit P0 (*rplp0*) were used. Primer sequences and concentrations were as follows: Telomere length (500 nM) forward, 5'-CGGTTTGTTTGGGTTTGGGTT TGGGTTTGGGTTTGGGTT-3' and reverse, 5'-GGCTTG CCTTACCCTTACCCTTACCCTTACCCTTACCCT-3' and single copy gene *rplp0* (250 nM) forward, 5'-CAGCAAGTG GGAAGGTGTAATCC-3' and reverse, 5'-CCCATTCTATCA TCAACGGGTACAA-3'. Thermocycling conditions for the telomere amplification were 90˚C for 10 min followed by 40 two-step PCR cycles of 95˚C for 15 sec and 60˚C for 10 sec. Results were analyzed using StepOne software v2.3 (Thermo Fisher Scientific, Inc.).

Cell cycle progression. Cell cycle distribution of LN-229 and LN PIN1 KO cells was evaluated by flow cytometry with propidium bromide. Both cell lines were seeded ($3x10^6$) in p100 plates in complete DMEM (Thermo Fisher Scientific, Inc.) with 10% FBS (Sigma Aldrich; Merck KGaA). Once 50-60% confluence was reached, the medium was replaced with fresh serum-free DMEM for 48 h at 37˚C to synchronize the cells. Following starvation, 10% FBS was added to only one plate for both lines; after 20 h at 37˚C, the cells were trypsinized, resuspended in 0.1% FBS-PBS, fixed in cold 70% v/v methanol for 30 min at -20˚C, treated with 1 μg/ml RNase A (Sigma Aldrich; MercK KGaA) and stained with propidium iodide (100 μg/ml) for 30 min at 37˚C protected from light. A total of $1x10^4$ events was recorded on a FACSCalibur (BD Biosciences) flow cytometer. Analysis was performed with FlowJo7.6.2 software (BD Biosciences).

Doubling time determination. A total of $1.5x10^4$ LN-229 and LN PIN1 KO cells was seeded in 24-well plates. Cells were cultured at 37˚C for 24, 48, 72 or 96 h. Then, cells were stained and fixed with crystal violet-methanol colorimetry method. Finally, cells were resuspended in ethanol:acetic solution (3:1) and measured at 570 nm. Duplication time was calculated using exponential growth phase values by comparing non-linear fit curves using GraphPad Prism 6 software (GraphPad Software, Inc.).

Cell migration. LN-229 and LN PIN KO cells were cultured in DMEM with 10% FBS to 60-70% confluence and then washed with PBS. Fresh serum-free DMEM was added; 24 h post-starvation, cells were resuspended using Dissociation Buffer (Gibco; Thermo Fisher Scientific, Inc.) and were manually counted and incubated for 30 min at 37˚C for recovery. For migration assay, Transwell insert plates with 8.0 μm membrane (Guangzhou Jet Bio-Filtration Co., Ltd.) were used. A total of 500 μl DMEM with 10% FBS was added to the lower chamber and 300 μl serum-free medium was added to the upper chamber containing $1.5x10^5$ cells. The plate was incubated at 37˚C. After 20 h, cells were fixed for 10 min with methanol solution and stained for 15 min with crystal violet solution, both at room temperature. Migration was quantified by direct manually counting under an inverted light microscope (Leica Microsystems, Inc.) with magnification of x100.

Evaluation of senescence induction. Senescence-associated β-galactosidase (SA-β-gal) activity was measured in LN-229 and LN PIN1 KO cells. Fixation and staining were performed using the Senescence β-galactosidase Staining Kit (Cell Signaling Technology, Inc.) according to the manufacturer's instructions. SA-β-gal-positive cells were manually counted in four randomly selected fields/well under an inverted light microscope (Leica Microsystems) at a magnification of 100x.

Evaluation of apoptosis induction. Apoptosis in protein lysates of LN-229 and LN PIN1 KO cells was determined through Caspase 3 activity measurement using CaspACE™ Assay System, according to the manufacturer's instructions (Promega Corporation).

Animals. A total of 20 8-week-old (weight, 20 g) inbred athymic and immunocompetent BALB/c AnN N:NIH(S)-nu female mice were purchased from National University of La Plata (Buenos Aires, Argentina) and, after randomization to LN-229 (n=10) and LN PIN1 KO (n=10), were housed (5 mice/cage). Mice were housed at constant temperature (24˚C) and relative humidity (40%), under a 12/12-h light/dark schedule. Food and water were supplied *ad libitum*. The general health of the animals was monitored daily. The present protocol was approved by the Institutional Commission for the Care and Use of Laboratory Animals (approval no. CICUAL UNQ 011-15).

Tumor progression. LN-229 and LN PIN1 KO cells were collected by trypsinization once they reached 80% confluence in monolayer culture. Cells were manually quantified by hemocytometer and resuspended in RPMI medium (Thermo Fisher Scientific, Inc.). After 30 min at 37˚C, the cell suspension was mixed with Vitrogel (TheWell Bioscience, Inc.) in a 2:3 ratio. A 250 μl mixture containing $5x10^6$ cells was injected into nude mice subcutaneously. The following day, in order to establish the starting tumor volume, the remaining volume of injection with Vitrogel was determined. During a 69-day follow-up period, the size of tumors was measured twice/week. The shortest and longest diameters of tumors were measured using a caliper and tumor volume was calculated as follows: Tumor volume (mm^3)=(longest diameter) x (shortest diameter)^2 x0.5 (29). The tumor progression was assessed twice with 5 animals/experimental group.

Mice were anaesthetized with 5% isoflurane and sacrificed by cervical dislocation when tumor volume reached 1,000 mm^3 If the indicated volume was not reached after 69 days, the mice were sacrificed as humane endpoint. The animals were necropsied in order to excise tumors, which were fixed overnight in 4% Paraformaldehyde at room temperature and embedded in paraffin at 50˚C for 8 h. Tumors were stored at room temperature for subsequent histological analysis.

Histological analysis. The fixed tumors were cut into 5-μm-thick sections, which were deparaffinized. The sections were stained at room temperature with hematoxylin (Biopack) for 5 min, soaked in tap water for 5 min, and counterstained for 3 min with eosin (Biopack). Color brightfield images of hematoxylin and eosin (H&E)-stained tumor sections were acquired using Cytation 5 Cell Imaging Multi-Mode Reader

(BioTek Instruments Inc.) at 2.5x magnification. Images were collected using a 4x5 grid and stitching was performed with the Image Montage function of the Gen5 Image software (BioTek Instruments Inc.) setting a tile overlap of 10%.

Necrotic area. The necrotic area in tissue stitched images was measured with ImageJ 1.5p Software (30). Tumor necrosis was identified as sections with increased eosinophilia; quantification of both necrotic and viable tissue was performed using the 'Color Threshold' tool, setting the units in μm using the scale bar in each image as reference.

Mitosis. H&E-stained tissue sections were analyzed for mitotic count calculation. Mitotic figures in all basic stages of mitosis were manually counted using a high-power field (magnification, x400) and 10 images/experimental group.

Statistical analysis. All data are presented as the mean ± SEM (n=3). Comparisons between >2 was performed using one-way ANOVA followed by post hoc Tukey's multiple comparisons test. For two groups, differences were determined by unpaired Student's t or Mann-Whitney test as appropriate. The analysis was performed using GraphPad Prism 6 (GraphPad Software, Inc.; Dotmatics). P<0.05 was considered to indicate a statistically significant difference.

Results

Validation of PIN1 KO. To assess PIN1 KO by CRISPRCas9, PIN1 levels were determined in control and transfected LN-229 cells using western blotting and flow cytometry. In western blotting and flow cytometry analysis PIN 1 was not detected on LN PIN1 KO cell line (Fig. 1A and B, respectively). Thus, successful induction of LN PIN1 KO was confirmed.

PIN1 KO inhibits NF-κB pathway signaling. As previously described, NF-κB pathway signaling promotes proliferation and invasion in GBM (15). A GBM model showed that decreased PIN1 levels inhibits the NF-κB pathway (15); therefore, the present study evaluated the status of this signaling pathway in LN PIN1 KO cells. A commercial plasmid that contains a promoter sequence recognized by active NF-κB associated with a reporter gene was used. In LN PIN1 KO cells, active levels of NF-κB decreased significantly in comparison with LN-229 cells (Fig. 2A).

PIN1 KO reduces both htert and IL-8 gene expression. As PIN1 has been reported to regulate *htert* and *IL-8* gene expression by NF-κB activation (15,22), the relative expression of both genes was quantified by the ΔΔCq method using *β-actin* as endogenous loading control. The relative gene expression of *htert* and *IL-8* was significantly decreased by 50% in LN PIN1 KO cells compared with LN-229 cells (Fig. 2B and C).

LN PIN1 KO cells exhibit decreased telomerase activity. Due to changes observed in *htert* transcription levels, it was hypothesized that LN PIN1 KO cells would exhibit lower telomerase activity. Using RQ-TRAP assay, a significant drop to 44.5% telomerase activity was confirmed in LN PIN1 KO cells compared with its parental cell line LN-229 (Fig. 3A).

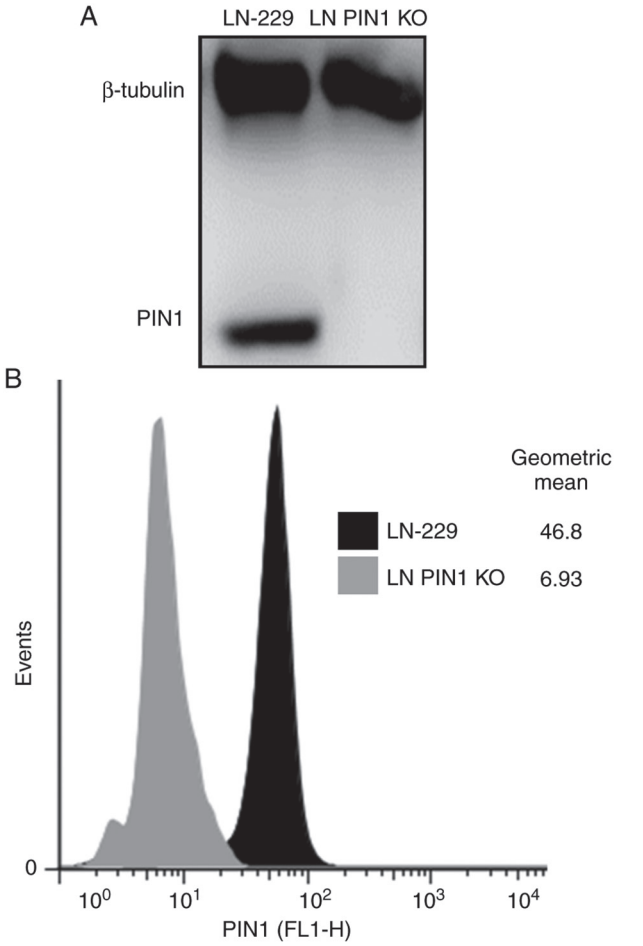

Figure 1. LN PIN1 KO cells do not express PIN1 protein. (A) Protein lysate of LN-229 and LN PIN1 KO cells was analyzed by western blot to determinate PIN1 expression. PIN1 levels were determined by densitometry using LI-COR Image Studio™. *β-tubulin* was used as loading control. (B) Flow cytometry histogram of both cell lines labelled with the anti-PIN1 antibody. KO, knock out.

PIN1 KO induces telomere shortening. Relative telomeric length in both cell lines was determined by qPCR with specific primers for the telomeric sequence and *rplp0* gene for normalization. LN PIN1 KO cells underwent telomeric shortening, showing a significant decrease of 47.04% in length of their telomeres after at least 9 passages (Fig. 3B).

Proliferation decreases in LN PIN1 KO cells. The present study evaluated the impact of PIN1 KO on cell cycle progression by flow cytometry. The percentage of cells in each phase of the cell cycle was determined. A significant difference was observed in response to FBS stimulus; LN PIN1 KO cells showed a lower response to FBS stimulus than the parental cell line LN-229 (Fig. 4B).

The percentage of cells in G0-G1 phase increased by 67.9% in LN PIN1 KO cells compared with LN-229. Furthermore, the percentage of LN PIN1 KO cells in S and G2-M phases decreased by 75.00 and 63.34%, respectively, compared with LN-229 (Fig. 4A and B). Additionally, PIN1 induces expression

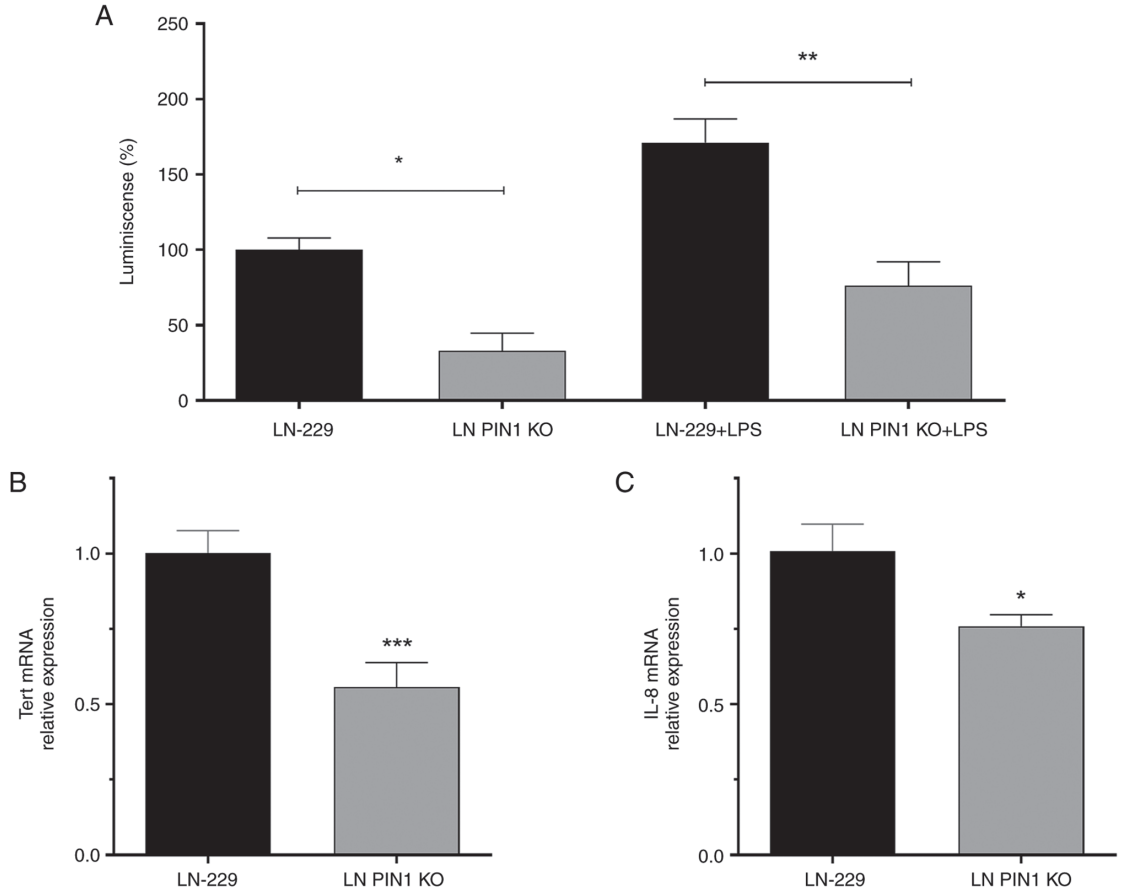

Figure 2. Determination of NF-κB pathway status following PIN1 KO. (A) Determination of NF-κB pathway activation levels by luminescence assay in LN-229 and LN PIN1 KO cells transfected with pHAGE-NFKB-TA-LUC-UBC-tdTomato-W. *P<0.05, **P<0.01. Data were analyzed by one-way ANOVA with Tukey's multiple comparisons test. (B) Relative expression of (B) *IL-8* and (C) *htert* gene in LN-229 and LN PIN1 KO cells. Reverse transcription-quantitative PCR was performed using endogenous control *β-actin*. Data were analyzed by two-tailed unpaired Student's t test. Data are presented as the mean ± SEM (n=3). *P<0.05, ***P<0.001 vs. LN-229. KO, knockout; htert, human telomerase reverse transcriptase.

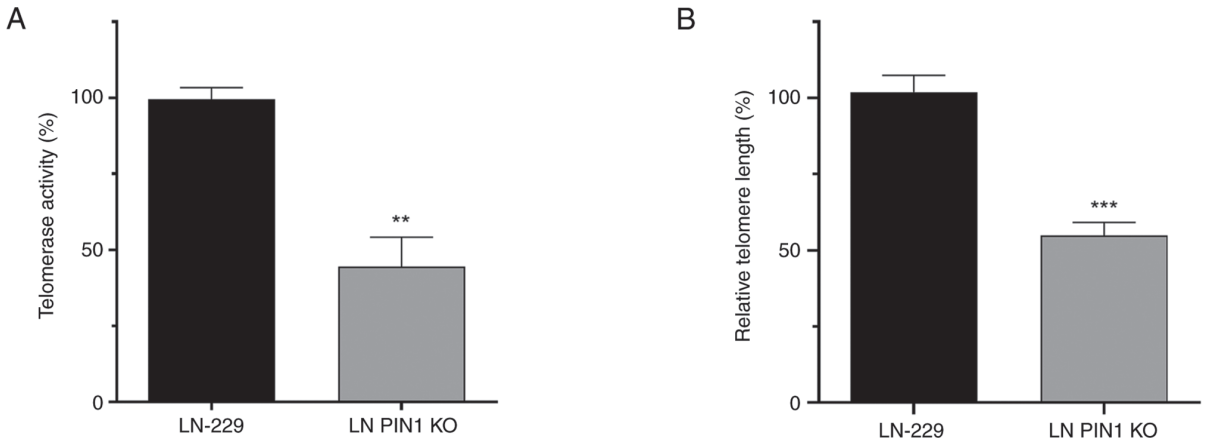

Figure 3. PIN1 role in telomeric homeostasis. (A) Determination of telomerase activity by real-time quantitative telomerase repeat amplification protocol assay. Quantification was performed by real-time PCR with specific primers using as template protein lysate obtained from LN-229 and LN PIN1 KO. (B) Quantification of telomere length was performed by reverse transcription-quantitative PCR with specific primers using as template genomic DNA from LN-229 and LN PIN1 KO cells. Data were analyzed by two-tailed unpaired Student's t test. Values represent the mean ± SEM (n=3). **P<0.01, ***P<0.001 vs. LN-229. KO, knockout.

of Cyclin D1, a key cell cycle regulator (31,32). Therefore, levels of cyclin D1 were evaluated. A significant decrease in Cyclin D1 mRNA and protein levels were determined for LN PIN1 KO compared with LN-229 cells (Fig. 4C and D).

LN PIN1 KO increases cell doubling time. As PIN1 is involved in cell cycle regulation (31,32), the effect of PIN1 KO on cell doubling time was determined (Fig. 5A). For LN PIN1 KO, a higher mean doubling time of 47.13 h was

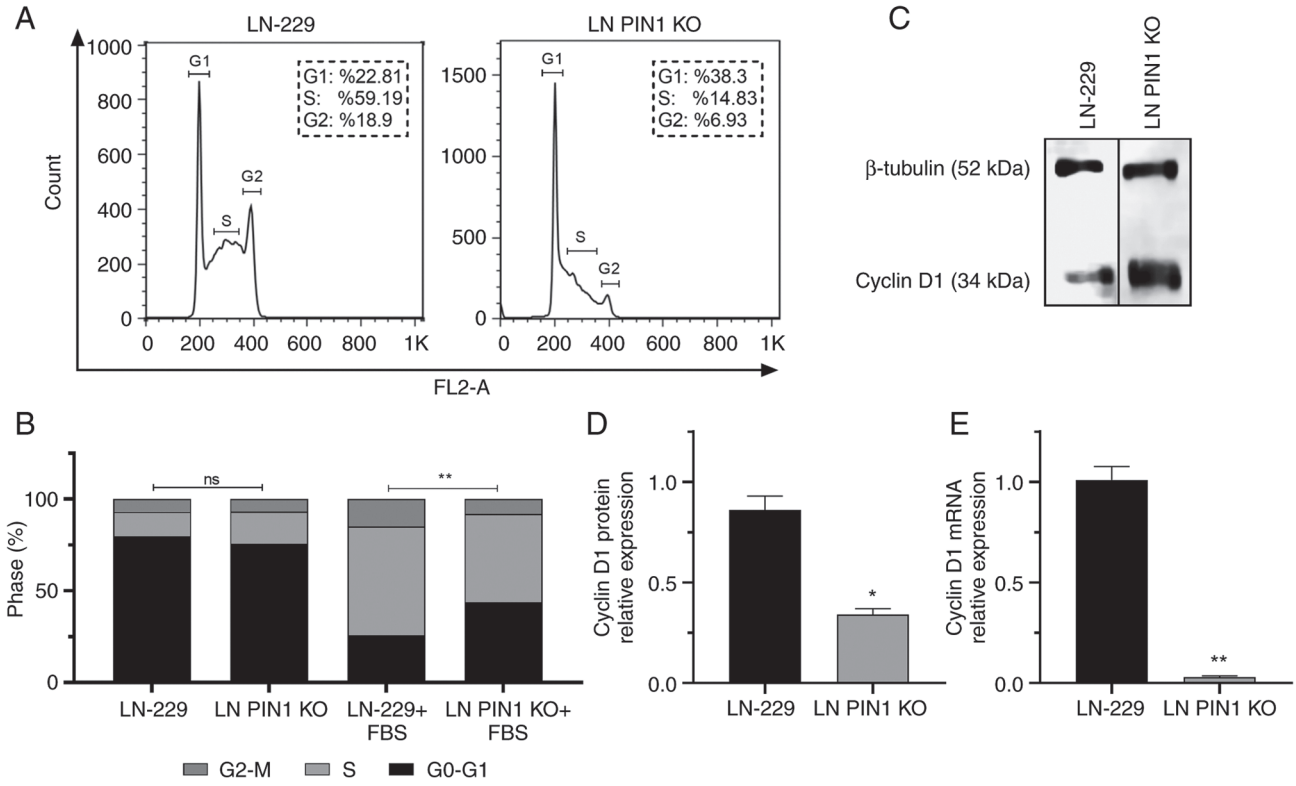

Figure 4. LN PIN1 KO cells exhibit lower proliferative response to FBS. Representative graphs of three independent cell cycle experiments by propidium iodide staining and flow cytometry. (A) Histograms corresponding to FBS-induced cells. (B) Cell percentages for each cell cycle stage in starved control and starved + FBS induction groups. Data were analyzed by one-way ANOVA (n=3). **P<0.01. (C) Protein lysates of LN-229 and LN PIN1 KO cells were analyzed by western blot to determine Cyclin D1 expression. β-tubulin was used as loading control. (D) Cyclin D1 protein expression levels were determined by densitometry using LI-COR Image Studio™. (E) Relative expression of cyclin D1 gene in LN-229 and LN PIN1 KO cells by reverse transcription-quantitative PCR using β-actin as endogenous control. Data were analyzed by two-tailed unpaired Student's t test. Values represent the mean ± SEM (n=3). *P<0.05, **P<0.01 vs. LN-229. KO, knockout; ns, not significant.

obtained, in comparison with LN-229 doubling time which was 34.6 h.

PIN1 KO reduces cell migration. Given the key role of PIN1 importance in cell migration (17), the LN PIN1 KO cell migratory capacity was evaluated using Transwell assays. The migratory capacity of the PIN1 KO cells decreased to 28.04% compared with LN22-9 cells (Fig. 5Ba and b).

PIN1 KO induces senescence and apoptosis. The role of PIN1 in senescence and apoptosis was evaluated. The percentage of senescent cells was calculated using the Senescence β-Gal Staining kit. The mean stained LN-229 cells/field was 1.97%; LN PIN1 KO exhibited ~53.46% β-gal-positive cells (Fig. 5C).

To evaluate whether PIN1 KO triggers apoptosis, caspase 3 activity was measured by CaspACE Assay System apoptosis kit. LN PIN1 KO cells showed a significant 46.4% increase in Caspase 3 activity compared with LN-229 (Fig. 5D).

PIN1 KO decreases tumorigenic potential in vivo. Finally, a nude mouse xenograft model was established to validate the functional effect of PIN1 KO. Tumors in control mice injected with the LN-229 cells grew significantly at day 52 (data not shown); however, the LN PIN1 KO group showed no notable tumor growth throughout the trial. In addition, the difference in tumor volume of both groups was significant starting at day 47 (Fig. 6A). Since Vitrogel is not completely reabsorbed, a threshold of 400 mm^3 was used to determine tumor incidence (data not shown). The LN-229 group generated tumors between days 41 and 52, while 100% of the group inoculated with the LN PIN1 KO remained tumor free to the final of the protocol on day 69. Finally, on day 69 tumor volumes were calculated. Tumors in the LN-229 group presented a mean volume of 1,018 mm^3; mean volume for the group inoculated with LN PIN1 KO was 152.4 mm^3, (Figs. 6B and S1).

LN PIN KO inhibits tumor development. H&E staining was used to examine histological features of tumors generated by both cell lines. While LN-229 tumors showed marked hypercellularity, large necrotic foci area and high mitotic cell count (Fig. 6Ca and b), tumors corresponding to LN PIN KO cells showed lower cell density and a decrease in mitotic cell count (Fig. 6Cc and d). LN-229 cell tumors exhibited a mean necrotic area of 17.22%; necrotic area in LN PIN1 KO cell tumors was 10.12% (Fig. 6D). The mean mitotic cells/field for LN PIN1 KO was 0.32; for LN-229, the mean was significantly higher at 7.18 (Fig. 6D). Overall LN PIN1 KO tumors presented a less proliferative phenotype than tumors obtained from the parental cell line LN-229.

Discussion

PIN1 serves a role in multiple types of cancer due to its ability to interact with several signaling pathways and regulate a

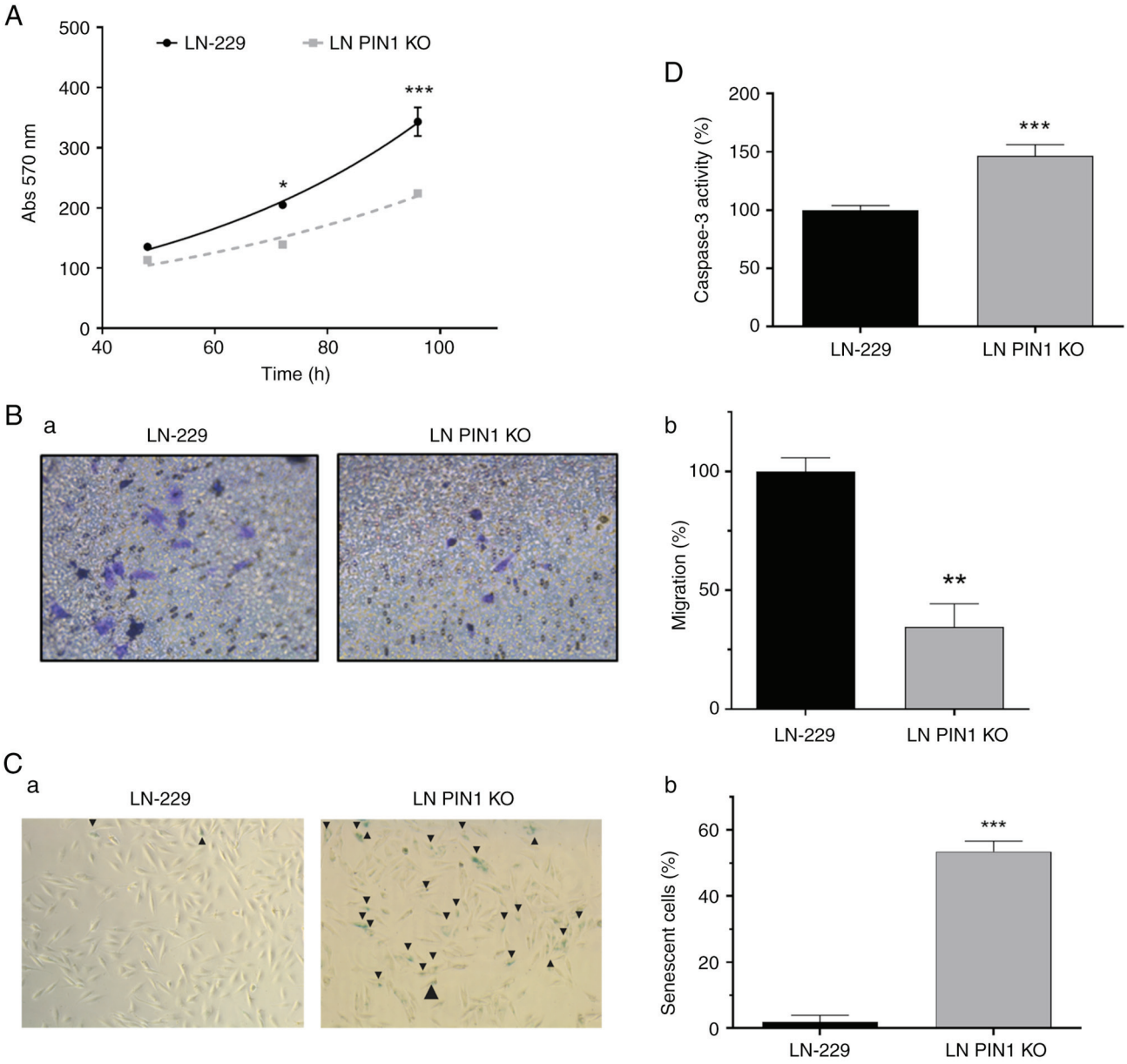

Figure 5. PIN1 KO significantly modifies glioblastoma cell line behavior. (A) PIN1 KO increases the doubling time of the cells. Cells were fixed and counted with crystal violet colorimetry method and measured at 570 nm. Doubling time was calculated in exponential phase of growth using GraphPad Prism 6 software. Data are presented as the mean ± SEM (n=3). *P<0.05, ***P<0.001. (B) LN PIN1 KO decreases cell migration. (Ba) Representative images of Transwell migration assay stained with violet crystal (magnification, x100). (Bb) Relative cell migration. Data were analyzed by two-tailed unpaired Student's t test. **P<0.01 vs. LN-229. (C) PIN1 KO significantly increases the number of senescent cells. (Ca) Determination of senescence-associated β-galactosidase activity by Senescence β-Galactosidase Staining kit (magnification, x100). Black arrows indicate senescent cells. (Cb) Percentage of positive β-galactosidase cells was quantified by direct counting of four fields of vision/well. Data are presented as the mean ± SEM (n=3). ***P<0.0001 vs. LN-229. (D) Increased apoptosis in LN PIN KO cells. Apoptosis levels were determined by caspase 3 activity. Data were analyzed by two-tailed unpaired student's t test. Values represent the mean ± SEM (n=3). ***P<0.001 vs. LN-229. KO, knockout; Abs, absorbance.

wide range of cellular processes linked to tumor development and progression (7,33,34). PIN1 is highly expressed in most types of cancer and increased PIN1 expression is usually associated with poorer cancer prognosis (12). Although the full role of PIN1 activity in cancer remains to be defined, several molecular mechanisms associated with PIN1 activity, including regulation of different transcription factors responsive to growth-inducing signals, have been described (35-37). These underlying mechanisms result in enhanced proliferative signaling, resistance to cancer cell death, replicative immortality and invasion and metastasis (35). PIN1 has also been associated with glioma genesis and progression since it is involved in pro-survival mechanisms, increased invasion and angiogenic potential. In addition, PIN1 has been reported to provide metabolic advantages to glioma cells (36,38,39). PIN1 is expressed in glioma stem-like cells (GSCs) and its silencing or inhibition abrogates GSC viability and mitigates GSC-driven tumor progression (40). Therefore, PIN1 has emerged as an attractive molecular target for development of novel treatments in GBM. Thus, the aim of the present work was to determine the role of PIN1 in a GBM model to postulate it as a novel target for treatment of this disease.

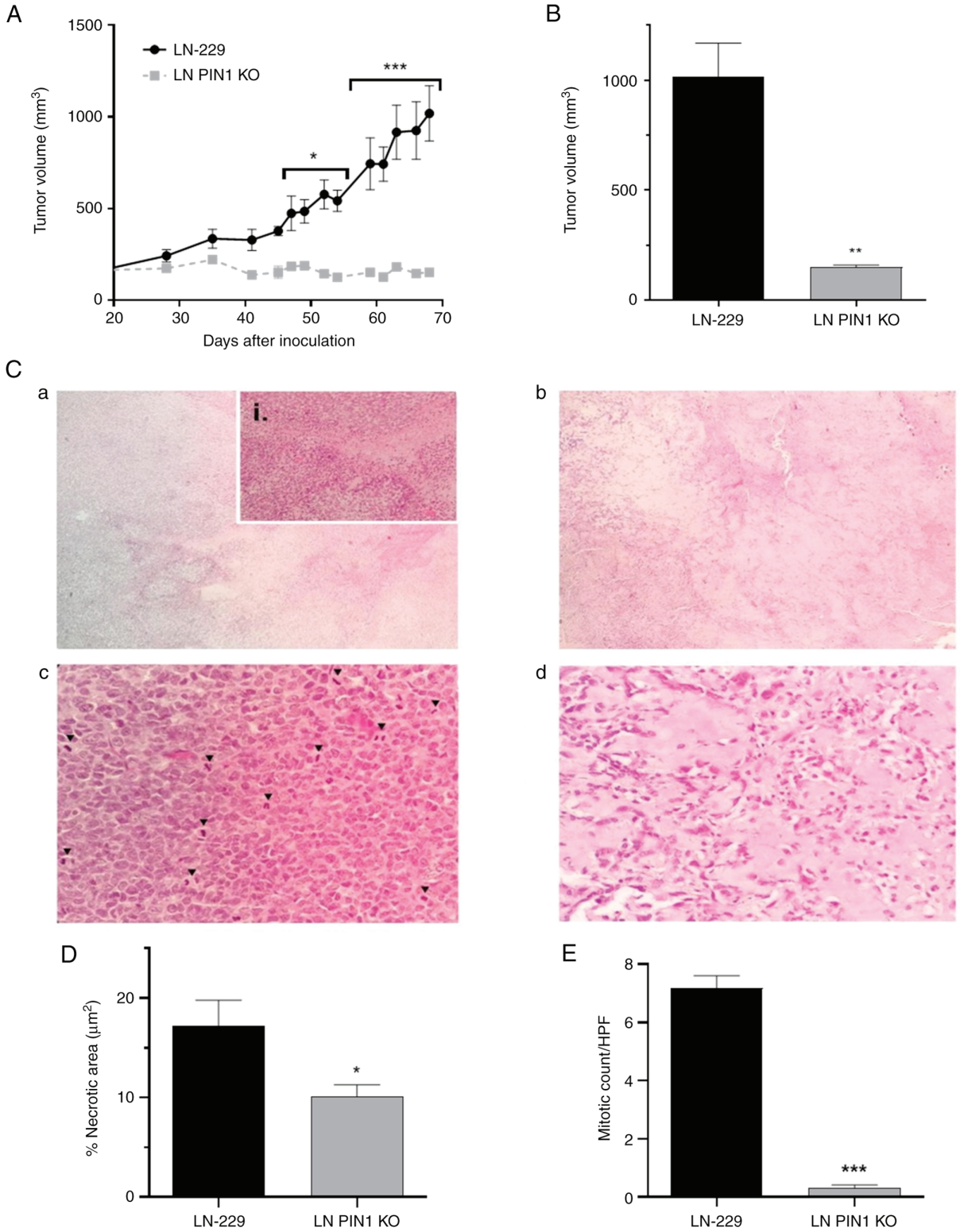

Figure 6. Loss of PIN1 suppresses tumor growth *in vivo*. Representative graphs from two independent experiments of *in vivo* tumor progression. (A) Tumor growth. n=4. ***P<0.001. (B) Final tumor volume. Data were analyzed by two-tailed unpaired student's t test. Values represent the mean ± SEM (n=5). **P<0.01 vs. LN-229. (C) Representative tissue sections from LN-229 and LN-229 PIN1 KO xenografts at 40x (Ca and Cc) and 400x (Cb and Cd) magnification following hematoxylin and eosin staining. (Ca) LN-229 group presented serpentine patterned necrotic foci with (Cai) pseudopalisades in the periphery, high cellularity and (Cb) increased mitotic activity (arrowhead). (Cc) Diffuse necrotic areas were observed in LN PIN1 KO tumors. (Cd) Viable tissue showed scarce mitotic bodies and a low cellular density. (D) Necrotic area relative to the total tumor area. (E) Mitotic cell count by HPF. Data were analyzed by two-tailed unpaired Student's t test. Data represent the mean ± SEM (n=3). *P<0.05; ***P<0.001 vs. LN-229. KO, knockout; HPF, high-power field.

PIN1-targeted small molecule compounds have already been described (35). Juglone is a pharmacological inhibitor of PIN1 but its potential application for cancer treatment is limited due to specificity issues (41,42). Additionally, other inhibitory molecules have been described, such as PiB (43) and KPT-6566 (44), that show a promising clinical application.

United States Food and Drug Administration-approved all-trans retinoic acid (ATRA) acts as a PIN1 inhibitor in acute promyelocytic leukemia and breast cancer (45). Further, combination therapy with ATRA and arsenic trioxide (ATO) has shown a cooperative effect affecting primarily PIN1 activity (46). These pharmacological inhibitors demonstrate that PIN1 is a feasible target for cancer therapy; validation studies are key to establish which types of cancer may benefit from this therapeutic approach.

KO model generation for specific genes is a widely employed tool in basic research to validate a gene of interest as a molecular target (47,48). CRISPR/Cas9 facilitates both identification and validation of new molecular targets for specific drug development and provides a rapid method to generate KO cell and animal models (49).

The present study used CRISPR/Cas9 to construct a LN PIN1 KO cell model and validate PIN1 as a molecular target. PIN1 protein was not detected in PIN1 KO cell lysate by western blot analysis, indicating successful model construction by CRISPR/Cas9. This result was verified by evaluation of PIN1 expression by flow cytometry, where no PIN1 signal was observed in LN PIN1 KO cells.

To the best of our knowledge, the present study is the first to use a PIN1 KO cell model in GBM to investigate the roles of PIN1 in this disease. By using this model, PIN1 involvement in telomere maintenance and oncogenic behavior in GBM were studied by comparing KO cells with the LN-229 cell line. The present work comprises a single cell line of GBM. Future studies should use a larger cell line panel and patient-derived cells to confirm PIN1 role in GBM. Nevertheless, the results of the present study contribute to evidence of the role of PIN1 in GBM.

PIN1 inhibition decreases activation of NF-κB pathway signaling and its effectors in a GBM cell model (15). One of the genes regulated by this pathway is *htert*, which serves a key role in replicative immortality by promoting telomere elongation in tumor cells (50). PIN1 enhances *htert* expression by activating NF-κB in GBM, as seen in another disease model (22). PIN1 inhibition may be involved in telomere maintenance in GBM, not only by TRF1 modulation but also by altering htert expression and telomerase activity. The results obtained support this hypothesis: The present study evaluated the active levels of NF-κB in LN PIN1 KO cells and observed that PIN1 KO promoted inhibition of this pathway, as seen in another GBM cell model (15). Here, *htert* transcription also decreased significantly in LN PIN1 KO cells.

Here, decreased *htert* expression was observed to trigger a decrease in activity of the holoenzyme telomerase, which generates progressive telomere shortening in the PIN1 KO cell model. Therefore, it was hypothesized that this telomeric imbalance, generated by PIN1 deletion, contributes to the entry of LN PIN1 KO cells into senescence and cell apoptosis. However, telomere shortening may not be the only process mediated by PIN1 that generates senescence and apoptosis considering that this protein also regulates cell cycle progression and survival signals (34).

Here, LN PIN1 KO cells presented a longer doubling time, with an increase of almost 40% compared with LN-229 cells. This was consistent with cell cycle analysis: LN PIN1 KO cells showed cell cycle arrest in G0-G1 phase. This was due at least in part to decreased Cyclin D1 levels in LN PIN1 KO cells (as indicated by western blot and RT-qPCR analysis).

GBM presents an invasive phenotype that is one of the characteristics of this type of tumor that hinder its treatment at the clinical level (32). PIN1 has also been reported to promote migration in different tumor types, including GBM (33). It has been reported that the activation of NF-κB promotes migration in GBM via the expression of *IL-8* (15,51). The present model exhibited a decrease in the active levels of NF-κB; therefore levels of *IL-8* transcription were evaluated, as well as the migratory capacity of LN PIN1 KO cells. LN PIN1 KO cells exhibited a decrease in *IL-8* transcription and migratory capacity compared with LN-229 cells.

Here, PIN1 deletion also appears to suppress the ability to form tumors *in vivo* in a murine xenogeneic model. Compared with LN-229 cells, xenografts generated from LN PIN1 KO cells grew at a markedly slower rate and some tumors did not progress from their initial volume. These results were consistent with histological analysis of the tumors, where LN-229 cells showed a high percentage of necrotic area accompanied by high cellularity and mitotic body count. All these features are typical histological characteristics of developed GBM tumors (2). By contrast, these aspects were not observed in LN PIN1 KO group, suggesting a higher number of senescent and/or apoptotic cells. Similar results have been reported in other tumors, where depletion or inhibition of PIN1 leads to modulation of cellular processes, such as cell migration, cell cycle progression and *in vivo* tumor growth (2,13,52).

Taken together, the results of the present study show the contribution of PIN1 in telomeric regulation and other key cellular processes for development and tumor progression in GBM. Although the ability of PIN1 to regulate telomeres via TRF1 has been reported (21), to the best of our knowledge, the present results support a novel mechanism that involves regulation of *htert* expression and lower telomerase activity.

In summary, loss of PIN1 in LN-229 cells leads to decreased malignant behavior and tumorigenicity, both *in vitro* and *in vivo*, supporting a key role of PIN1 in the present GBM model. Furthermore, the present study demonstrated that the presence of PIN1 affects telomeric dynamics by downregulating *htert* expression and telomerase activity in GBM. The present results provide a basis for design and development of new therapies for GBM based on PIN1 as a novel target for treatment of this disease.

Acknowledgements

The authors would like to thank Dr Fernanda Rubio (Molecular Biology and Apoptosis Laboratory, Medical Investigation Institute, UBA-CONICET, Buenos Aires, Argentina) for providing cyclin D1 antibody and Ms Isabel Cardoso (Molecular Oncology Unit, Center of Molecular and Translational Oncology, National University of Quilmes. Buenos Aires, Argentina) for technical support in qPCR and western blotting assays.

Funding

The present study was supported by Quilmes National University (grant no. PUNQ EXPTE 1297/19), the National

Agency for the Promotion of Science and Technology (grant no. PICT 2018 2372), Cancer National Institute (grant no. EXPTE 827-1533/18; Argentina) and Commission of Scientific Investigation from Buenos Aires (grant no. PDCT2022/GomezDE).

Availability of data and materials

The datasets used and analyzed during the current study are available from the corresponding author on reasonable request.

Authors' contributions

JM, GAC, DEG and DLMG designed the study. JM, RGA and LB performed *in vitro* experiments. JM and NTS performed *in vivo* experiments. JM, GAC, LB and DLMG wrote the manuscript. DEG and DLMG confirm the authenticity of all the raw data. All authors have read and approved the final manuscript.

Ethics approval and consent to participate

Animal experimentation protocol was approved by the Institutional Commission for the Care and Use of Laboratory Animals (approval no. CICUAL UNQ 011-15).

Patient consent for publication

Not applicable.

Competing interests

The authors declare that they have no competing interests.

References

1. Huttner A: Overview of primary brain tumors: Pathologic classification, epidemiology, molecular biology, and prognostic markers. Hematol Oncol Clin North Am 26: 715-732, 2012.
2. Louis DN, Perry A, Wesseling P, Brat DJ, Cree IA, Figarella-Branger D, Hawkins C, Ng HK, Pfister SM, Reifenberger G, *et al*: The 2021 WHO classification of tumors of the central nervous system: A summary. Neuro Oncol 23: 1231-1251, 2021.
3. Vredenburgh JJ, Desjardins A, Herndon JE II, Dowell JM, Reardon DA, Quinn JA, Rich JN, Sathornsumetee S, Gururangan S, Wagner M, *et al*: Phase II trial of bevacizumab and irinotecan in recurrent malignant glioma. Clin Cancer Res 13: 1253-1259, 2007.
4. Anjum K, Shagufta BI, Abbas SQ, Patel S, Khan I, Shah SAA, Akhter N and Hassan SSU: Current status and future therapeutic perspectives of glioblastoma multiforme (GBM) therapy: A review. Biomed Pharmacother 92: 681-689, 2017.
5. Zong H, Parada LF and Baker SJ: Cell of origin for malignant gliomas and its implication in therapeutic development. Cold Spring Harb Perspect Biol 7: a020610, 2015.
6. Bao L, Kimzey A, Sauter G, Sowadski JM, Lu KP and Wang DG: Prevalent overexpression of prolyl isomerase Pin1 in human cancers. Am J Pathol 164: 1727-1737, 2004.
7. Chen Y, Wu YR, Yang HY, Li XZ, Jie MM, Hu CJ, Wu YY, Yang SM and Yang YB: Prolyl isomerase Pin1: A promoter of cancer and a target for therapy. Cell Death Dis 9: 883, 2018.
8. Atabay KD, Yildiz MT, Avsar T, Karabay A and Kiliç T: Knockdown of Pin1 leads to reduced angiogenic potential and tumorigenicity in glioblastoma cells. Oncol Lett 10: 2385-2389, 2015.
9. Lu KP, Finn G, Lee TH and Nicholson LK: Prolyl cis-trans isomerization as a molecular timer. Nat Chem Biol 3: 619-629, 2007.
10. Takahashi K, Uchida C, Shin RW, Shimazaki K and Uchida T: Prolyl isomerase, Pin1: New findings of post-translational modifications and physiological substrates in cancer, asthma and Alzheimer's disease. Cell Mol Life Sci 65: 359-375, 2008.
11. Reichert M, Steinbach JP, Supra P and Weller M: Modulation of growth and radiochemosensitivity of human malignant glioma cells by acidosis. Cancer 95: 1113-1119, 2002.
12. Zhu Z, Zhang H, Lang F, Liu G, Gao D, Li B and Liu Y: Pin1 promotes prostate cancer cell proliferation and migration through activation of Wnt/β-catenin signaling. Clin Transl Oncol 18: 792-797, 2016.
13. Zhang Z, Yu W, Zheng M, Liao X, Wang J, Yang D, Lu W, Wang L, Zhang S, Liu H, *et al*: Pin1 inhibition potently suppresses gastric cancer growth and blocks PI3K/AKT and Wnt/β-catenin oncogenic pathways. Mol Carcinog 58: 1450-1464, 2019.
14. Farrell AS, Pelz C, Wang X, Daniel CJ, Wang Z, Su Y, Janghorban M, Zhang X, Morgan C, Impey S and Sears RC: Pin1 regulates the dynamics of c-Myc DNA binding to facilitate target gene regulation and oncogenesis. Mol Cell Biol 33: 2930-2949, 2013.
15. Atkinson GP, Nozell SE, Harrison DK, Stonecypher MS, Chen D and Benveniste EN: The prolyl isomerase Pin1 regulates the NF-kappaB signaling pathway and interleukin-8 expression in glioblastoma. Oncogene 28: 3735-3745, 2009.
16. Raychaudhuri B, Han Y, Lu T and Vogelbaum MA: Aberrant constitutive activation of nuclear factor kappaB in glioblastoma multiforme drives invasive phenotype. J Neurooncol 85: 39-47, 2007.
17. Wakabayashi K, Kambe F, Cao X, Murakami R, Mitsuyama H, Nagaya T, Saito K, Yoshida J and Seo H: Inhibitory effects of cyclosporin A on calcium mobilization-dependent interleukin-8 expression and invasive potential of human glioblastoma U251MG cells. Oncogene 23: 6924-6932, 2004.
18. Turner KJ, Vasu V and Griffin DK: Telomere biology and human phenotype. Cells 8: 73, 2019.
19. Armando RG, Mengual Gomez DL, Maggio J, Sanmartin MC and Gomez DE: Telomeropathies: Etiology, diagnosis, treatment and follow-up. Ethical and legal considerations. Clin Genet 96: 3-16, 2019.
20. Akincilar SC, Unal B and Tergaonkar V: Reactivation of telomerase in cancer. Cell Mol Life Sci 73: 1659-1670, 2016.
21. Lee TH, Tun-Kyi A, Shi R, Lim J, Soohoo C, Finn G, Balastik M, Pastorino L, Wulf G, Zhou XZ and Lu KP: Essential role of Pin1 in the regulation of TRF1 stability and telomere maintenance. Nat Cell Biol 11: 97-105, 2009.
22. Ghaffari SH, Momeny M, Bashash D, Mirzaei R, Ghavamzadeh A and Alimoghaddam K: Cytotoxic effect of arsenic trioxide on acute promyelocytic leukemia cells through suppression of NFkβ-dependent induction of hTERT due to down-regulation of Pin1 transcription. Hematology 17: 198-206, 2012.
23. Naderlinger E and Holzmann K: Epigenetic regulation of telomere maintenance for therapeutic interventions in gliomas. Genes (Basel) 8: 145, 2017.
24. Nasser MM and Mehdipour P: Exploration of involved key genes and signaling diversity in brain tumors. Cell Mol Neurobiol 38: 393-419, 2018.
25. Xiang X, Corsi GI, Anthon C, Qu K, Pan X, Liang X, Han P, Dong Z, Liu L, Zhong J, *et al*: Enhancing CRISPR-Cas9 gRNA efficiency prediction by data integration and deep learning. Nat Commun 12: 3238, 2021.
26. Livak KJ and Schmittgen TD: Analysis of relative gene expression data using real-time quantitative PCR and the 2(-Delta Delta C(T)) method. Methods 25: 402-408, 2001.
27. Armando RG, Gomez DM and Gomez DE: AZT exerts its antitumoral effect by telomeric and non-telomeric effects in a mammary adenocarcinoma model. Oncol Rep 36: 2731-2736, 2016.
28. Cawthon RM: Telomere measurement by quantitative PCR. Nucleic Acids Res 30: e47, 2002.
29. Tomayko MM and Reynolds CP: Determination of subcutaneous tumor size in athymic (nude) mice. Cancer Chemother Pharmacol 24: 148-154, 1989.
30. Schneider CA, Rasband WS and Eliceiri KW: NIH image to ImageJ: 25 Years of image analysis. Nat Methods 9: 671-675, 2012.
31. Nakashima M, Meirmanov S, Naruke Y, Kondo H, Saenko V, Rogounovitch T, Shimizu-Yoshida Y, Takamura N, Namba H, Ito M, *et al*: Cyclin D1 overexpression in thyroid tumours from a radio-contaminated area and its correlation with Pin1 and aberrant beta-catenin expression. J Pathol 202: 446-455, 2004.

32. Wulf GM, Ryo A, Wulf GG, Lee SW, Niu T, Petkova V and Lu KP: Pin1 is overexpressed in breast cancer and cooperates with Ras signaling in increasing the transcriptional activity of c-Jun towards cyclin D1. EMBO J 20: 3459-3472, 2001.
33. Wang J, Liu K, Wang XF and Sun DJ: Juglone reduces growth and migration of U251 glioblastoma cells and disrupts angiogenesis. Oncol Rep 38: 1959-1966, 2017.
34. Zhou XZ and Lu KP: The isomerase PIN1 controls numerous cancer-driving pathways and is a unique drug target. Nat Rev Cancer 16: 463-478, 2016.
35. Chuang HH, Zhen YY, Tsai YC, Chuang CH, Huang MS, Hsiao M and Yang CJ: Targeting Pin1 for modulation of cell motility and cancer therapy. Biomedicines 9: 359, 2021.
36. Pu W, Zheng Y and Peng Y: Prolyl isomerase Pin1 in human cancer: Function, mechanism, and significance. Front Cell Dev Biol 8: 168, 2020.
37. Cheng CW and Tse E: PIN1 in cell cycle control and cancer. Front Pharmacol 9: 1367, 2018.
38. Sang Y, Li Y, Zhang Y, Alvarez AA, Yu B, Zhang W, Hu B, Cheng SY and Feng H: CDK5-dependent phosphorylation and nuclear translocation of TRIM59 promotes macroH2A1 ubiquitination and tumorigenicity. Nat Commun 10: 4013, 2019.
39. Yang W and Lu Z: Nuclear PKM2 regulates the Warburg effect. Cell Cycle 12: 3154-3158, 2013.
40. Zhang A, Tao W, Zhai K, Fang X, Huang Z, Yu JS, Sloan AE, Rich JN, Zhou W and Bao S: Protein sumoylation with SUMO1 promoted by Pin1 in glioma stem cells augments glioblastoma malignancy. Neuro Oncol 22: 1809-1821, 2020.
41. Mesalam AA, El-Sheikh M, Joo MD, Khalil AAK, Mesalam A, Ahn MJ and Kong IK: Induction of oxidative stress and mitochondrial dysfunction by juglone affects the development of bovine oocytes. Int J Mol Sci 22: 168, 2020.
42. Paulsen MT and Ljungman M: The natural toxin juglone causes degradation of p53 and induces rapid H2AX phosphorylation and cell death in human fibroblasts. Toxicol Appl Pharmacol 209: 1-9, 2005.
43. Uchida T, Takamiya M, Takahashi M, Miyashita H, Ikeda H, Terada T, Matsuo Y, Shirouzu M, Yokoyama S, Fujimori F and Hunter T: Pin1 and Par14 peptidyl prolyl isomerase inhibitors block cell proliferation. Chem Biol 10: 15-24, 2003.
44. Campaner E, Rustighi A, Zannini A, Cristiani A, Piazza S, Ciani Y, Kalid O, Golan G, Baloglu E, Shacham S, *et al*: A covalent PIN1 inhibitor selectively targets cancer cells by a dual mechanism of action. Nat Commun 8: 15772, 2017.
45. Wei S, Kozono S, Kats L, Nechama M, Li W, Guarnerio J, Luo M, You MH, Yao Y, Kondo A, *et al*: Active Pin1 is a key target of all-trans retinoic acid in acute promyelocytic leukemia and breast cancer. Nat Med 21: 457-466, 2015.
46. Kozono S, Lin YM, Seo HS, Pinch B, Lian X, Qiu C, Herbert MK, Chen CH, Tan L, Gao ZJ, *et al*: Arsenic targets Pin1 and cooperates with retinoic acid to inhibit cancer-driving pathways and tumor-initiating cells. Nat Commun 9: 3069, 2018.
47. Chen S, Sun H, Miao K and Deng CX: CRISPR-Cas9: From genome editing to cancer research. Int J Biol Sci 12: 1427-1436, 2016.
48. Sánchez-Rivera FJ and Jacks T: Applications of the CRISPR-Cas9 system in cancer biology. Nat Rev Cancer 15: 387-395, 2015.
49. Lu Q, Livi GP, Modha S, Yusa K, Macarrón R and Dow DJ: Applications of CRISPR genome editing technology in drug target identification and validation. Expert Opin Drug Discov 12: 541-552, 2017.
50. Shalem-Cohavi N, Beery E, Nordenberg J, Rozovski U, Raanani P, Lahav M and Uziel O: The effects of proteasome inhibitors on telomerase activity and regulation in multiple myeloma cells. Int J Mol Sci 20: 2509, 2019.
51. Nagai S, Washiyama K, Kurimoto M, Takaku A, Endo S and Kumanishi T: Aberrant nuclear factor-kappaB activity and its participation in the growth of human malignant astrocytoma. J Neurosurg 96: 909-917, 2002.
52. Lian X, Lin YM, Kozono S, Herbert MK, Li X, Yuan X, Guo J, Guo Y, Tang M, Lin J, *et al*: Pin1 inhibition exerts potent activity against acute myeloid leukemia through blocking multiple cancer-driving pathways. J Hematol Oncol 11: 73, 2018.